Supplementary Information (SI) for Materials Horizons.
This journal is © The Royal Society of Chemistry 2024

Supporting Information

Significantly enhanced energy harvesting performance in lead-free piezoceramic via a synergistic design strategy

Jianxun Zhang,‡[a] Qianqian Xu,‡[a] Yan Zhang,[a] Wei Guo,*[b,c] Hanmin Zeng,[a] Yimeng He,[a] Jiatao Wu,[b,c] Longlong Guo,[b,c] Kechao Zhou,[a] Dou Zhang[a]*

[a] *State Key Laboratory of Powder Metallurgy, Central South University, Changsha, Hunan, 410083, China.*

[b] *School of Civil Engineering, Central South University, Changsha, Hunan, 410075, China.*

[c] *National Engineering Research Center of High-speed Railway Construction Technology, Changsha, Hunan, 410075, China.*

Email: yanzhangcsu@csu.edu.cn, guowei@csu.edu.cn

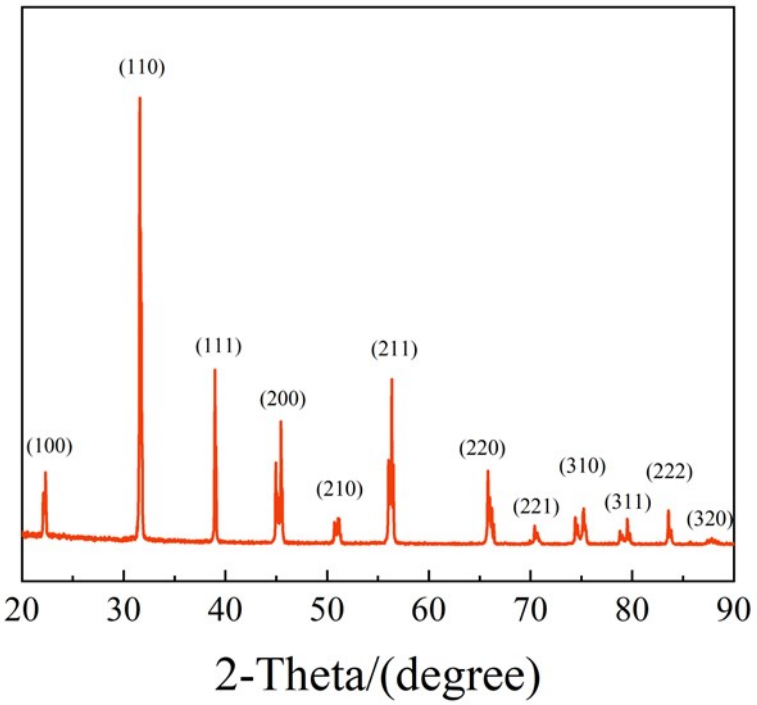

Fig. S1. XRD pattern of barium titanate powder.

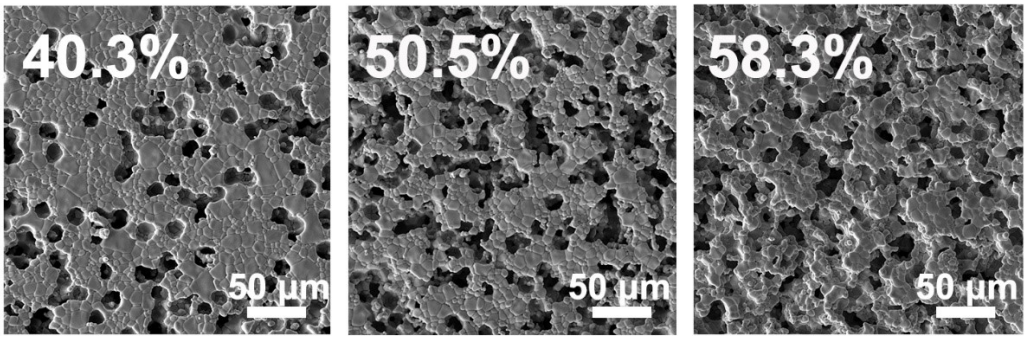

Fig. S2. SEM images (scale bar = 50 μm) of random porous BTO piezoceramics with porosity fraction of 40.3 %, 50.5 %, 58.3 %, respectively.

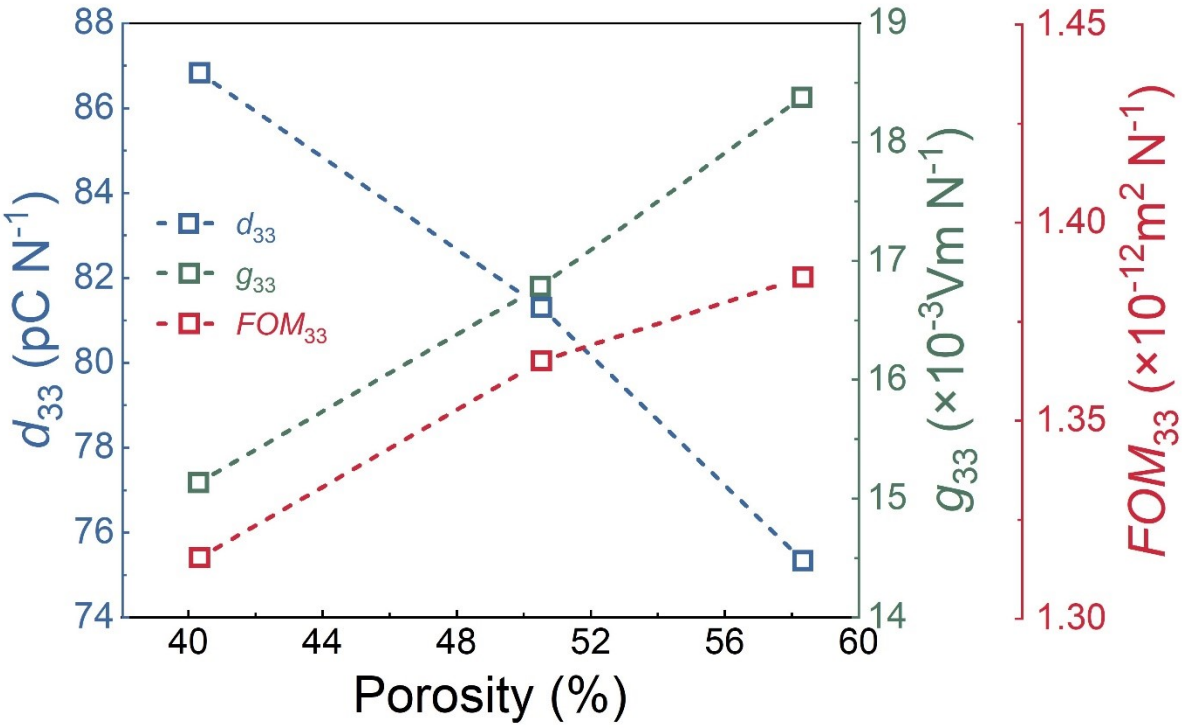

Fig. S3. Variation of piezoelectric coefficient (d_{33}), piezoelectric voltage coefficient (g_{33}) and piezoelectric energy harvesting figure of merit (FoM_{33}) for range of porosities of random porous ceramics.

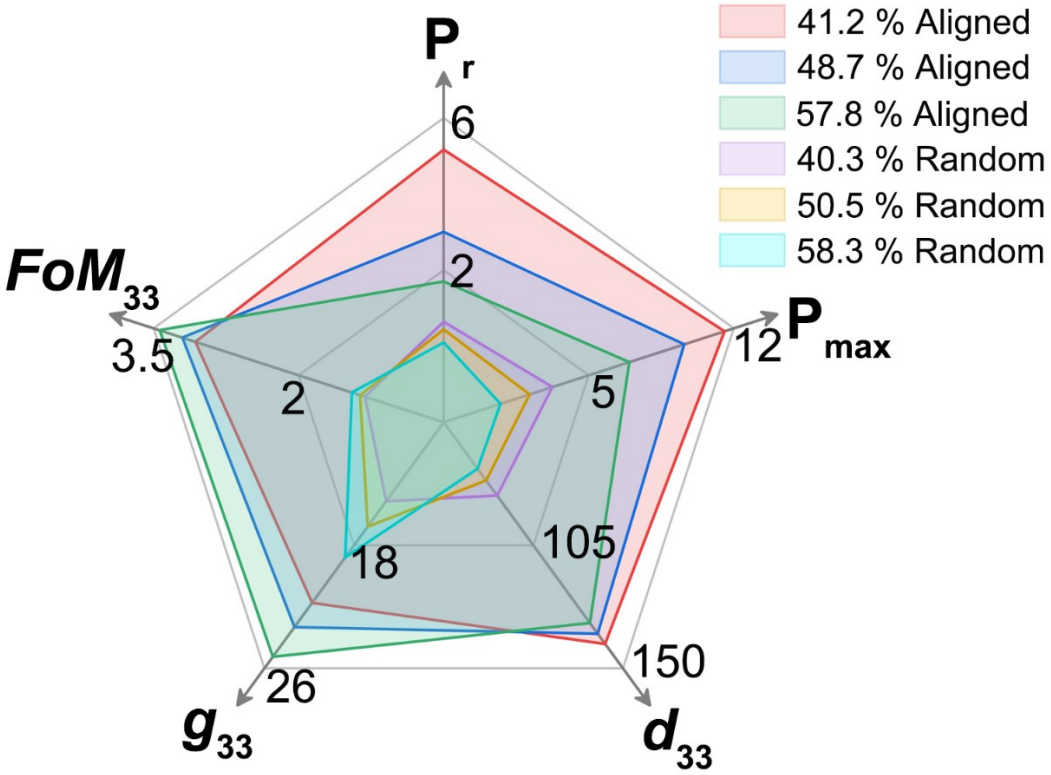

Fig. S4. Statistical diagram of electrical properties of BTO ceramics with different pore structures.

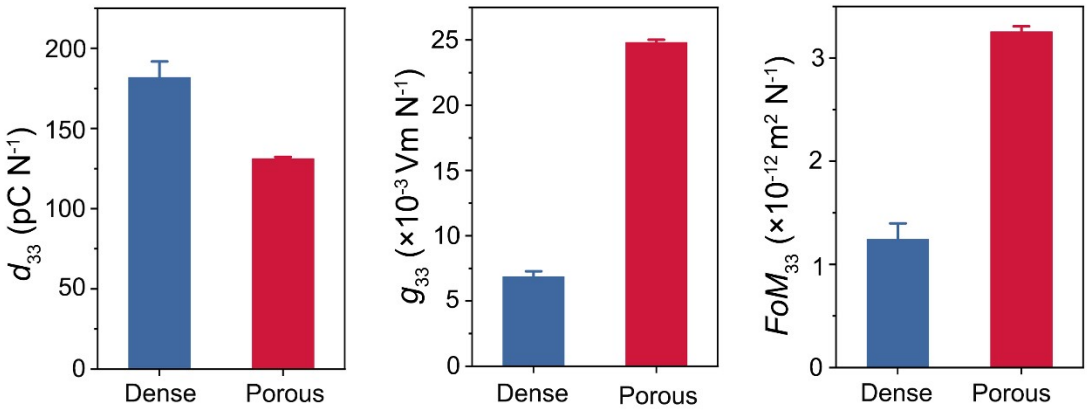

Fig. S5. The piezoelectric properties of aligned porous BTO ceramic (porosity fraction of 57.8 %) and dense BTO ceramic.

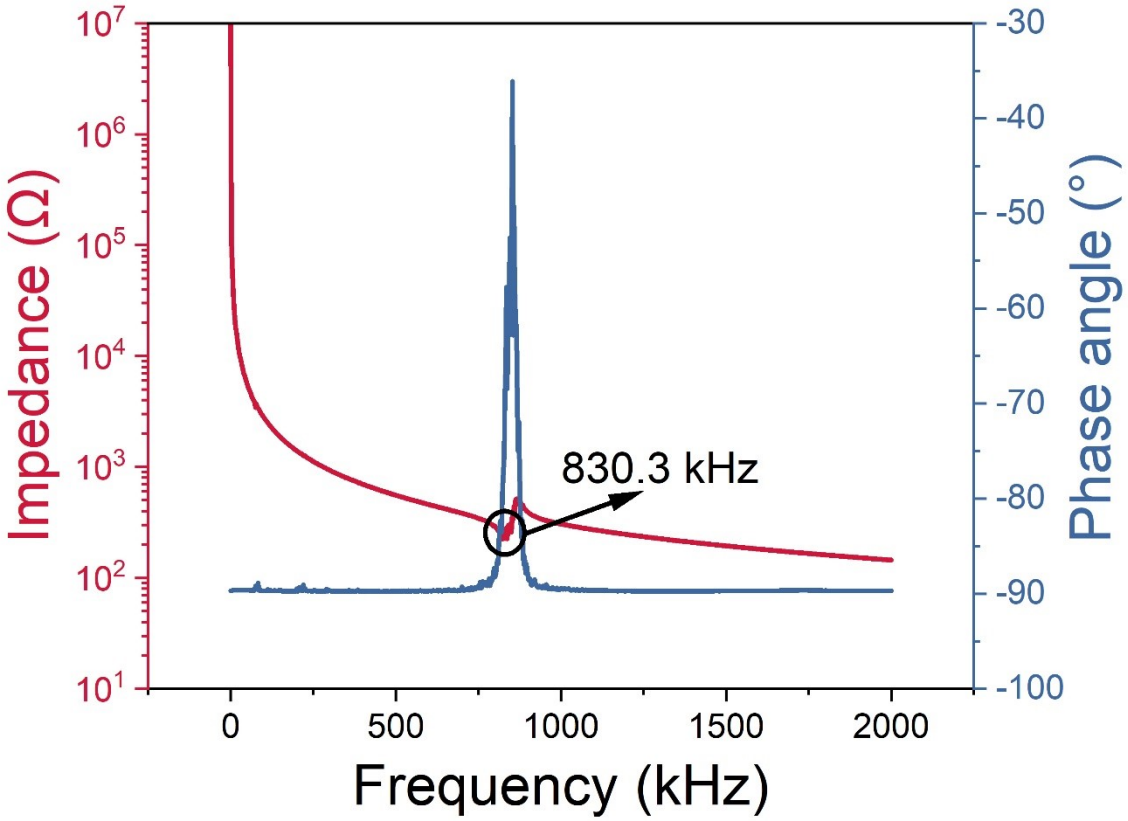

Fig. S6. The electric resonance frequency of the aligned porous BTO ceramics with 50 % porosity.

Fig. S7. Optical image showing 45 LEDs illuminated by piezoelectric energy harvester.

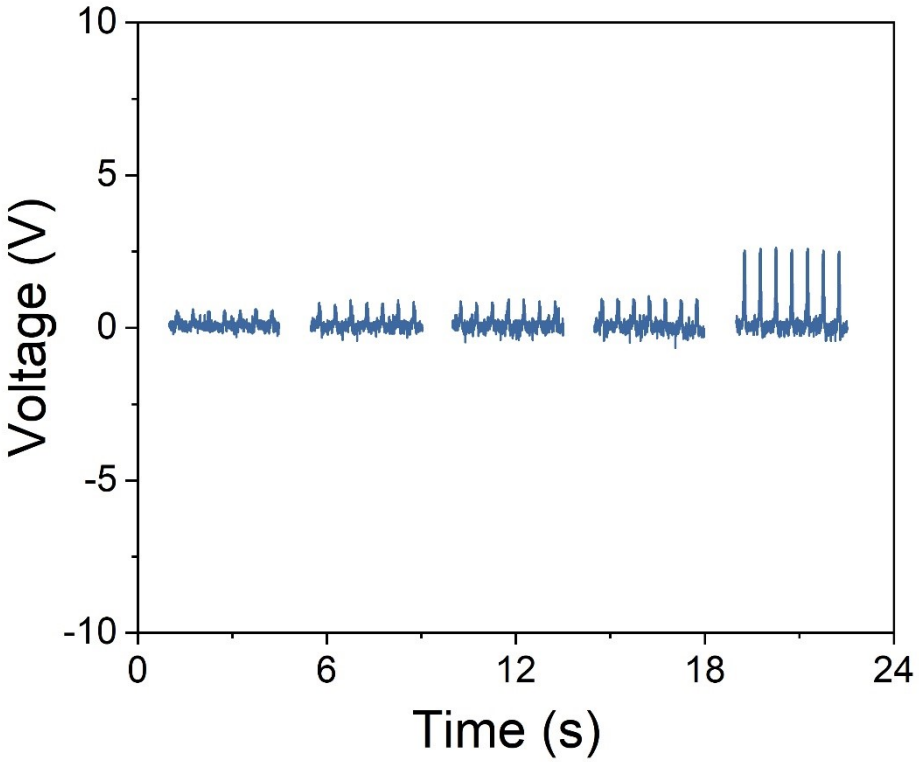

Fig. S8. Output voltage generated by non-polarized piezoelectric energy harvester.

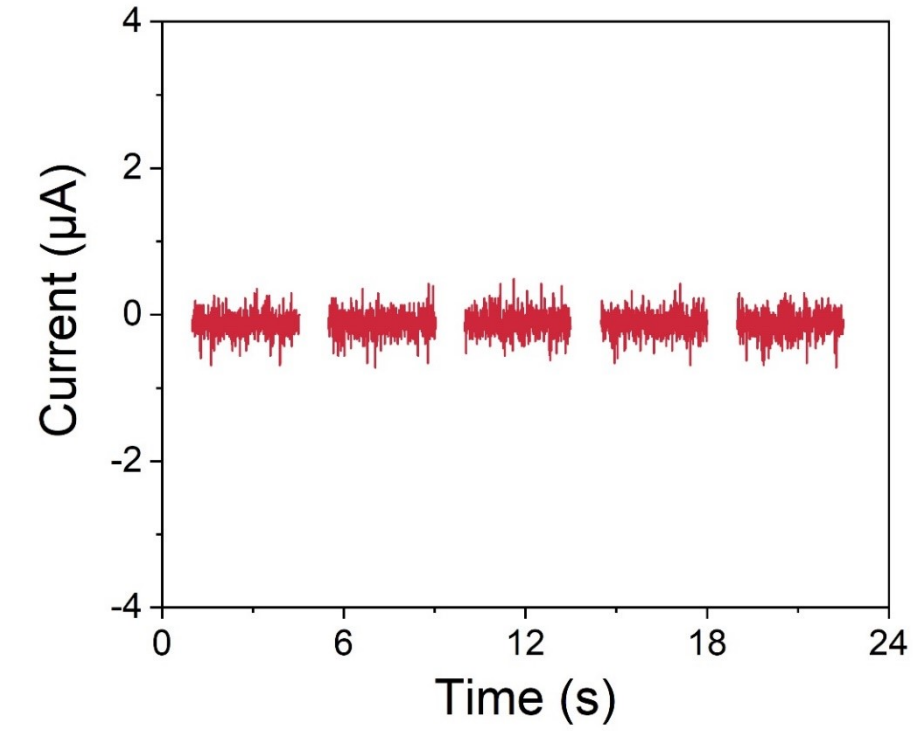

Fig. S9. Output current generated by non-polarized piezoelectric energy harvester.

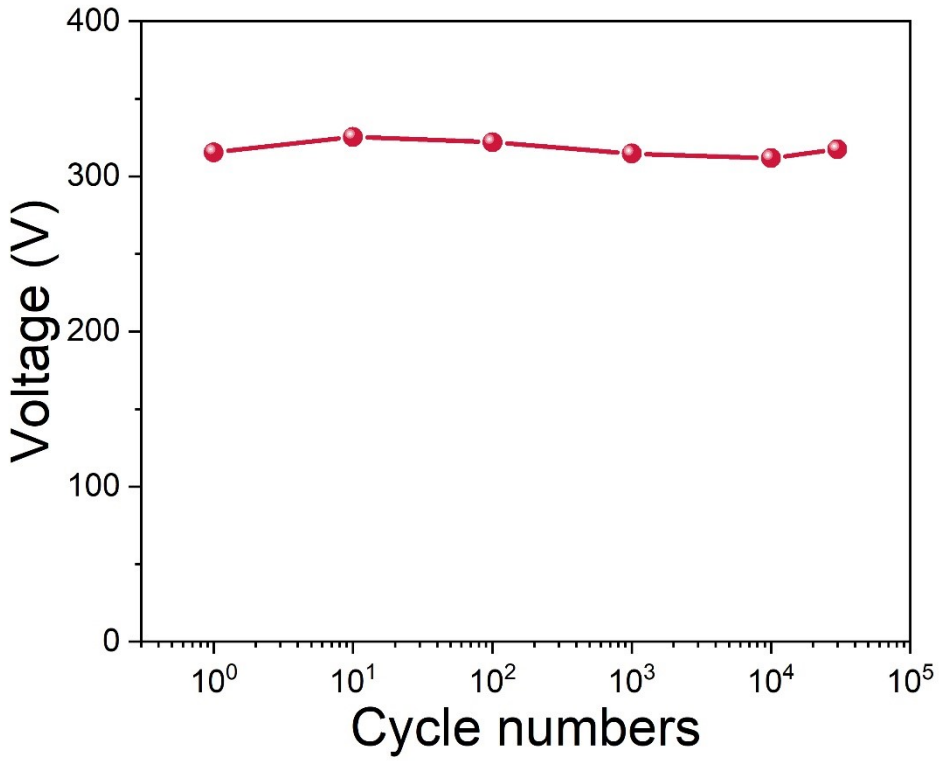

Fig. S10. The extended fatigue tests of the piezoelectric energy harvesters over 30,000 cycles.

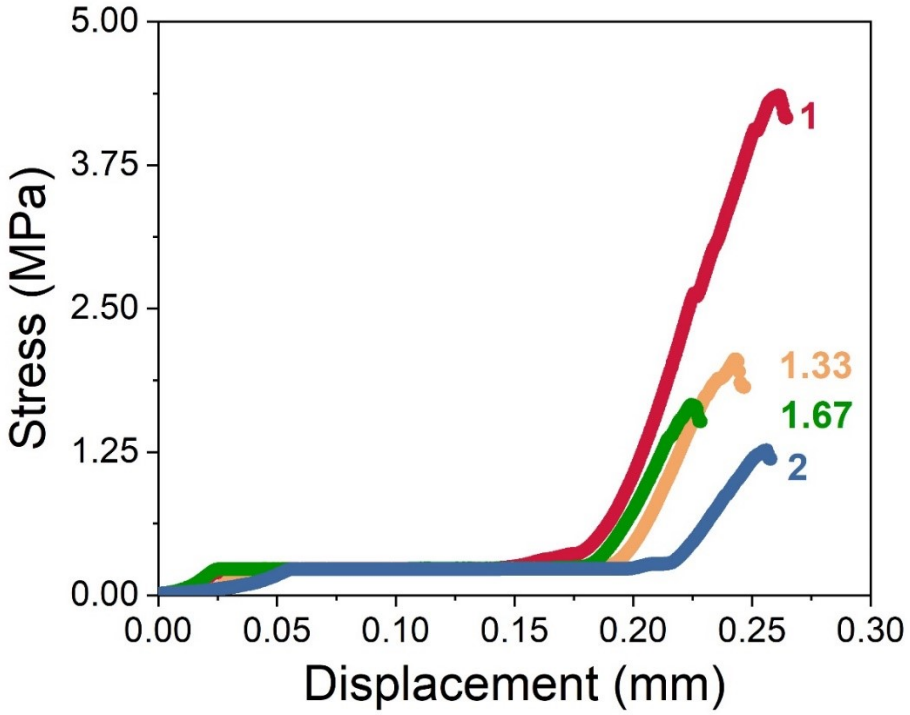

Fig. S11. Compressive stress with displacement for the piezoelectric energy harvesters with different aspect ratios.

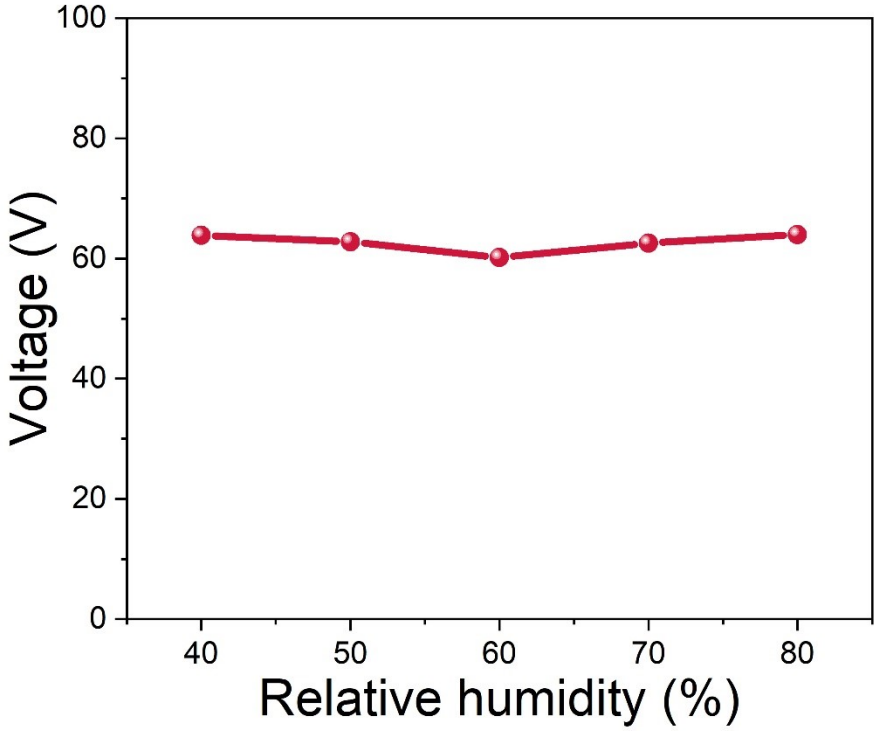

Fig. S12. The output voltage of the piezoelectric energy harvesters under different humidity conditions.

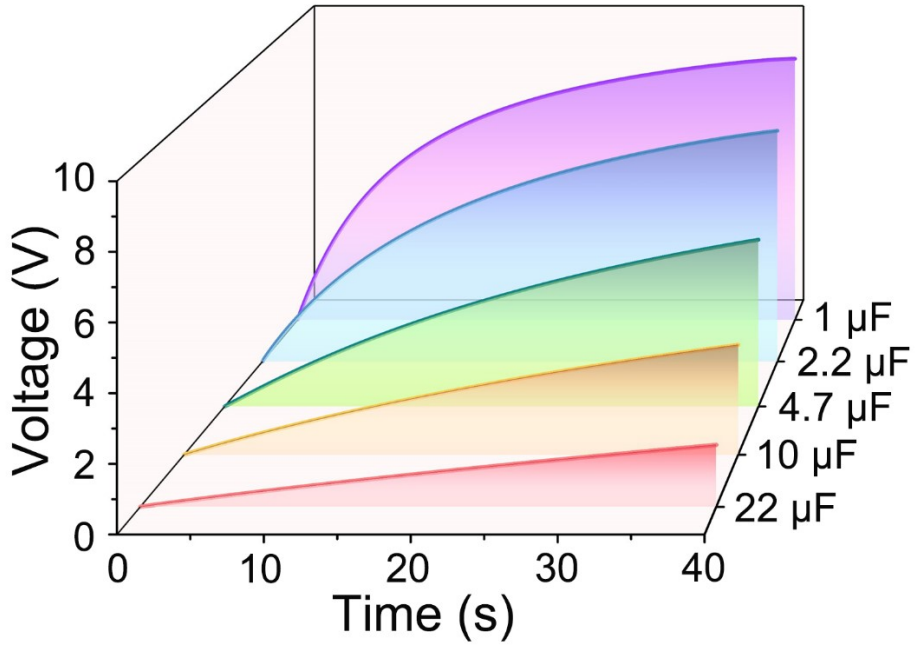

Fig. S13. Charging curves of the commercial capacitors (1, 2.2, 4.7, 10 and 22 μF) charged by piezoelectric energy harvester in 40 s.

Fig. S14. The digital photo of piezoceramic energy harvesters attached to a series of stainless-steel tubes.

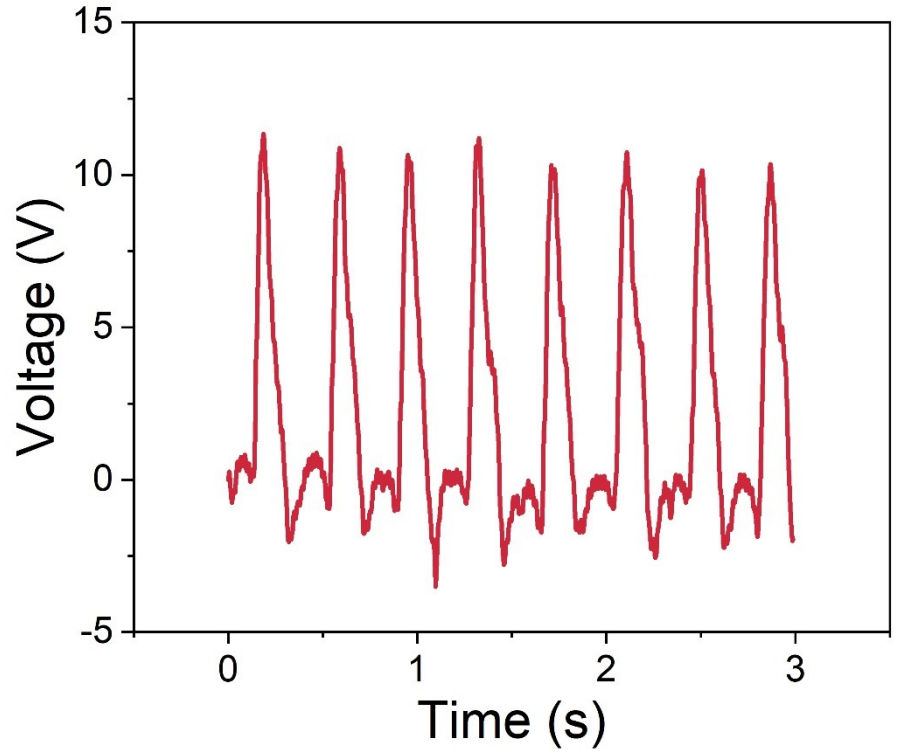

Fig. S15. Electrical signals generated by the piezoelectric energy harvester attached to wrists.

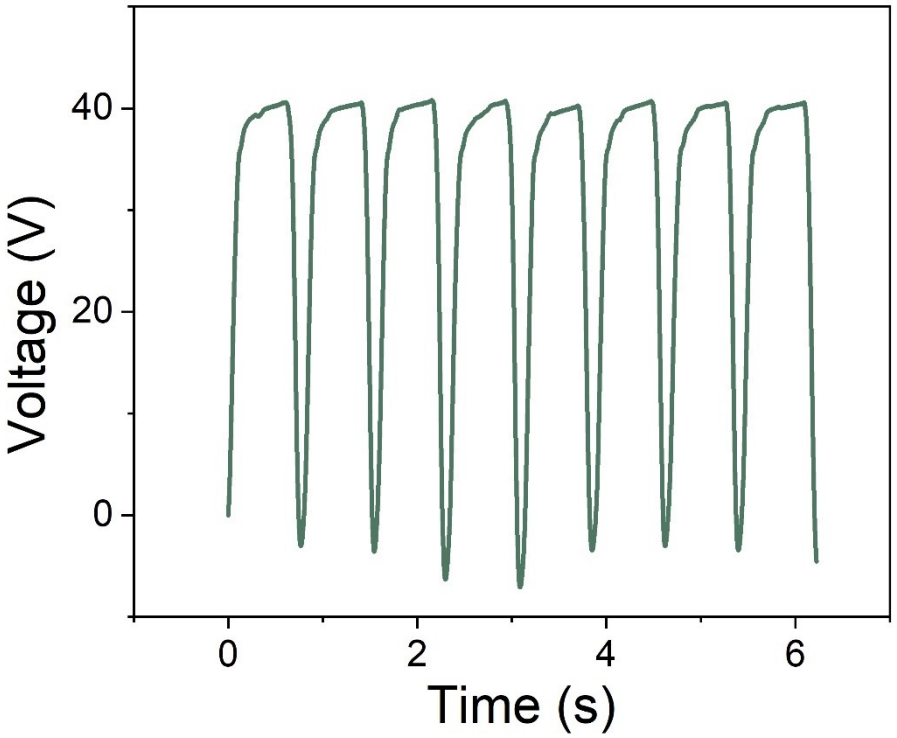

Fig. S16. Electrical signals generated by the piezoelectric energy harvester attached to fingers.

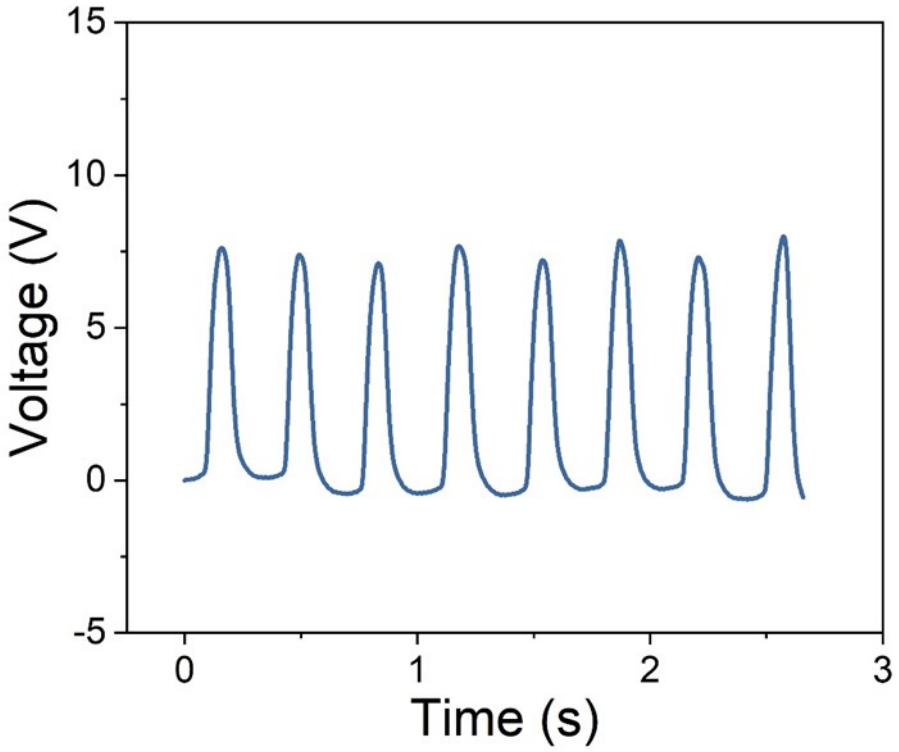

Fig. S17. Electrical signals generated by the piezoelectric energy harvester when tapped by fingers.

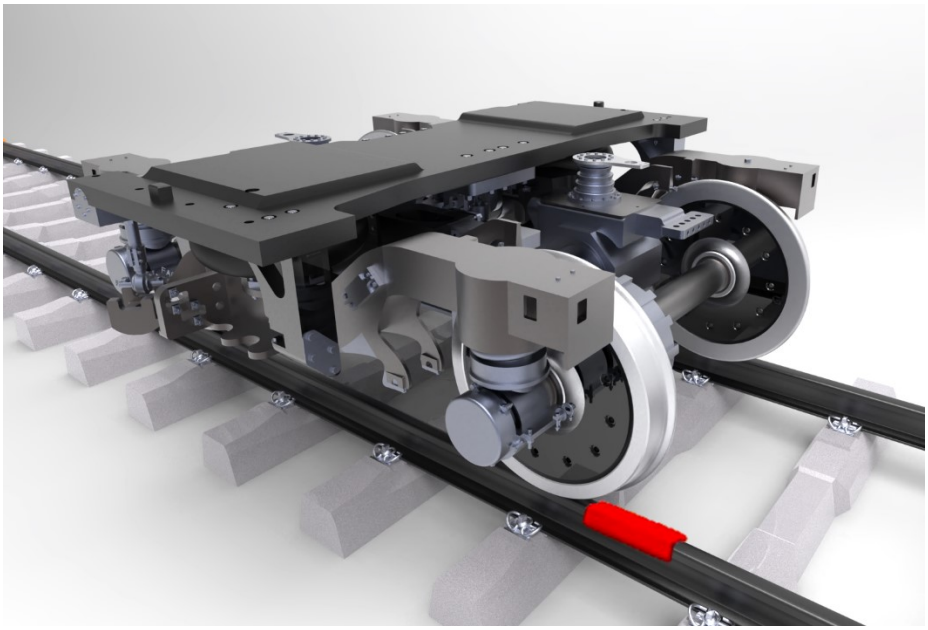

Fig. S18. Schematic of the bogie and the track when the train is about to pass the obstacle.

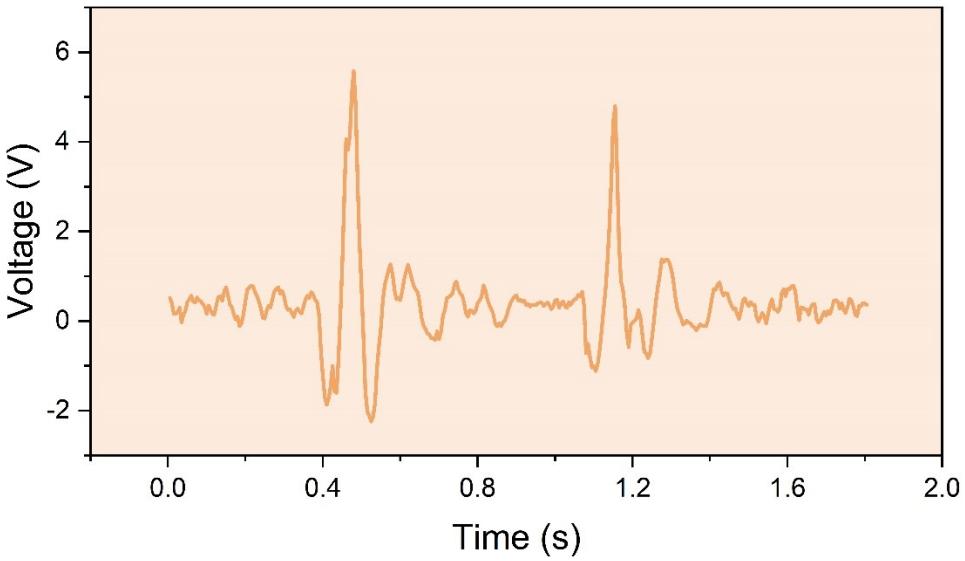

Fig. S19. Voltage response of the piezoelectric sensor when the right side of the train bogie pass obstacles

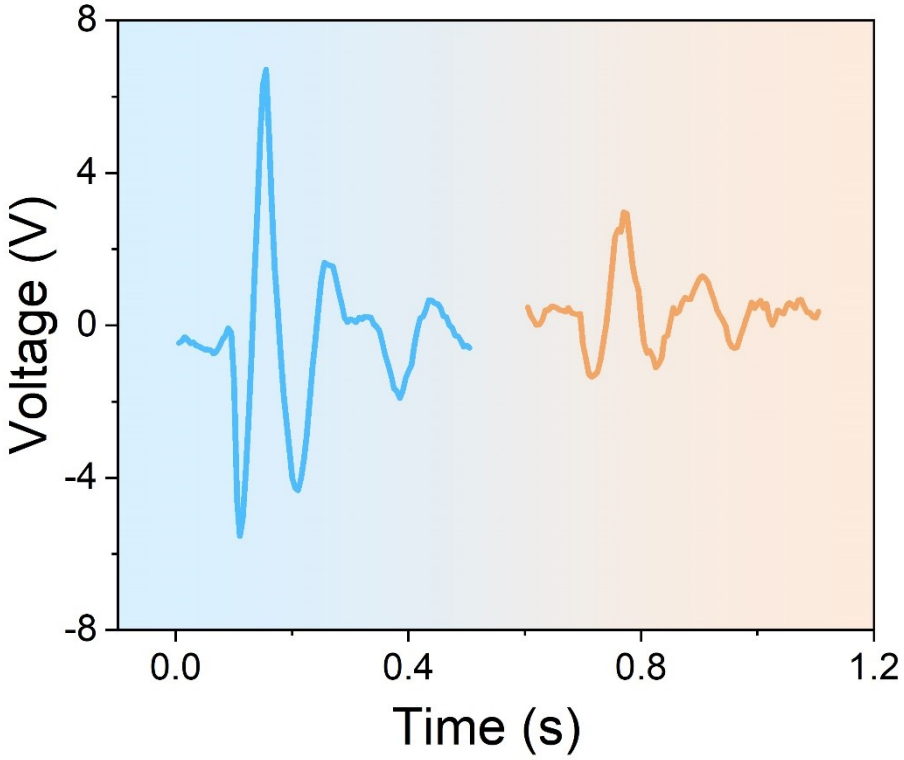

Fig. S20. Comparison of signals from the left and right sides of the train bogie pass obstacles.

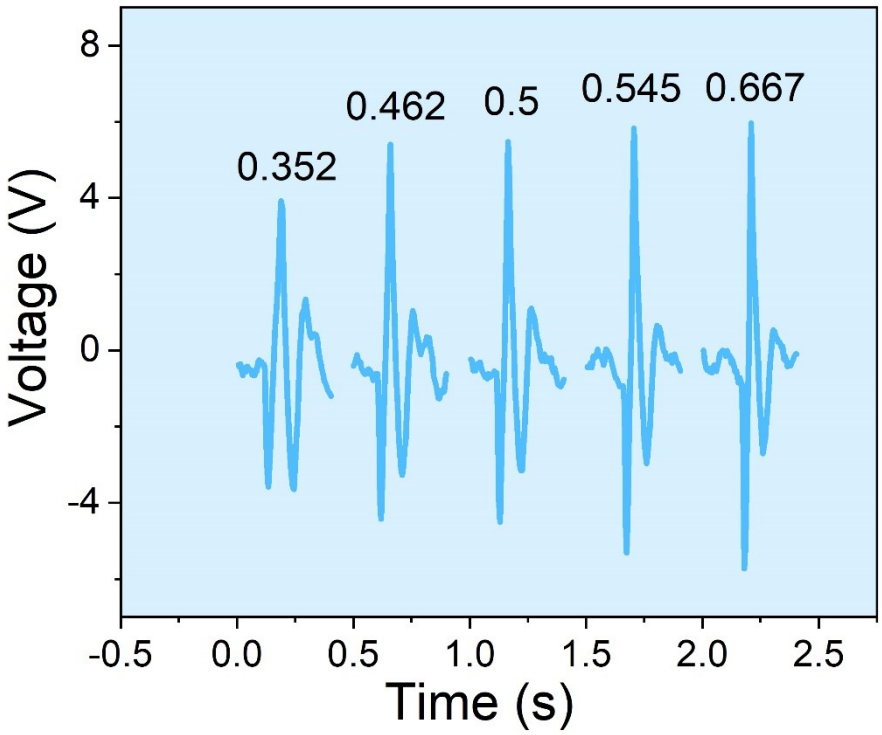

Fig. S21. Output voltage of the piezoelectric sensor applied in train monitoring at a train speed of 0.352, 0.462, 0.5, 0.545, 0.667 m s^{-1} and height of obstacle of 3 mm.

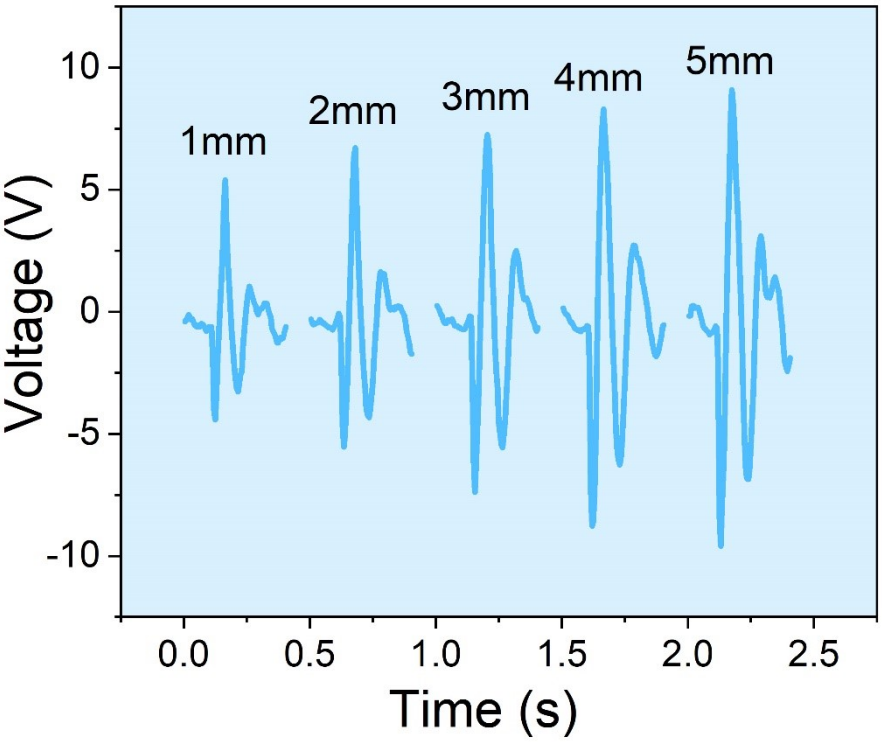

Fig. S22. Output voltage of the piezoelectric sensor applied in train monitoring at the height of obstacle of 1, 2, 3, 4, 5 mm and train speed of 0.462 m s^{-1}.

Table S1. Piezoelectric and dielectric properties of aligned porous ceramics with different porosity.

Porosity (%)	Relative permittivity	d_{33} (pC N^{-1})	g_{33} (10^{-3} V m N^{-1})	FoM_{33} ($\times10^{-12}$ m^2 N^{-2})
41.2	732.5	141.0	21.74	3.07
48.7	665.2	135.8	23.06	3.13
57.8	596.8	131.2	24.82	3.26

Table S2. Piezoelectric and dielectric properties of random porous ceramics with different porosity.

Porosity (%)	Relative permittivity	d_{33} (pC N^{-1})	g_{33} (10^{-3} Vm N^{-1})	FoM_{33} ($\times10^{-12}$ m^2 N^{-2})
40.3	647.9	86.8	15.13	1.32
50.5	547	81.3	16.79	1.37
58.3	463.5	75.3	18.38	1.39

Table S3. The results of finite element simulations of the piezoelectric energy harvesters with different aspect ratios.

Aspect ratio	Stress (N m^{-2})	Electric field (V)	Potential (V m^{-1})
1	1.57×10^6	1.89	1.26×10^4
1.33	1.64×10^6	2.08	1.72×10^4
1.67	2.18×10^6	2.14	2.74×10^4
2	2.95×10^6	2.19	3.43×10^4